AGU PUBLICATIONS

Geophysical Research Letters

RESEARCH LETTER
10.1002/2015GL064590

Key Points:
- Subglacial discharge produces seismic tremor
- Tremor allows for the first view of tidewater glacier discharge variations
- Despite fast flow, drainage efficiency of tidewater glaciers evolves seasonally

Supporting Information:
- Texts S1 and S2, Figures S1–S8, and Movie S1 caption
- Movie S1

Correspondence to:
T. C. Bartholomaus,
tbartholomaus@ig.utexas.edu

Citation:
Bartholomaus, T. C., J. M. Amundson, J. I. Walter, S. O'Neel, M. E. West, and C. F. Larsen (2015), Subglacial discharge at tidewater glaciers revealed by seismic tremor, *Geophys. Res. Lett.*, *42*, 6391–6398, doi:10.1002/2015GL064590.

Received 16 MAY 2015
Accepted 11 JUL 2015
Accepted article online 15 JUL 2015
Published online 10 AUG 2015

Subglacial discharge at tidewater glaciers revealed by seismic tremor

Timothy C. Bartholomaus[1], Jason M. Amundson[2], Jacob I. Walter[1], Shad O'Neel[3], Michael E. West[4], and Christopher F. Larsen[4]

[1]Institute for Geophysics, University of Texas at Austin, Austin, Texas, USA, [2]Department of Natural Sciences, University of Alaska Southeast, Juneau, Alaska, USA, [3]Alaska Science Center, U.S. Geological Survey, Anchorage, Alaska, USA, [4]Geophysical Institute, University of Alaska Fairbanks, Fairbanks, Alaska, USA

Abstract Subglacial discharge influences glacier basal motion and erodes and redeposits sediment. At tidewater glacier termini, discharge drives submarine terminus melting, affects fjord circulation, and is a central component of proglacial marine ecosystems. However, our present inability to track subglacial discharge and its variability significantly hinders our understanding of these processes. Here we report observations of hourly to seasonal variations in 1.5–10 Hz seismic tremor that strongly correlate with subglacial discharge but not with basal motion, weather, or discrete icequakes. Our data demonstrate that vigorous discharge occurs from tidewater glaciers during summer, in spite of fast basal motion that could limit the formation of subglacial conduits, and then abates during winter. Furthermore, tremor observations and a melt model demonstrate that drainage efficiency of tidewater glaciers evolves seasonally. Glaciohydraulic tremor provides a means by which to quantify subglacial discharge variations and offers a promising window into otherwise obscured glacierized environments.

1. Introduction

Subglacial discharge through tidewater glaciers links together several systems: it is produced primarily by glacier surface melt and rainfall; it travels englacially through conduits; it interacts with the subglacial bed and influences glacier velocities and erosion rates; and it is released into proglacial fjords where it raises sea levels and promotes fjord circulation, submarine melt, and marine productivity [*Motyka et al.*, 2006, 2013; *Chu*, 2013; *Sciascia et al.*, 2013; *Lydersen et al.*, 2014; *Slater et al.*, 2015]. Through its role as a critical link between ice-ocean systems, subglacial discharge modulates glacier and ice sheet change and resultant eustatic sea level rise [*Straneo et al.*, 2013]. Unfortunately, our understanding of the ice-water-ocean system has been limited by the challenge of making observations through kilometer-scale ice thicknesses and at the bottom of iceberg-choked fjords. Despite the long-standing prediction that subglacial discharge generates diagnostic seismic signals [*St. Lawrence and Qamar*, 1979], their detection remains fleeting and rare [*Winberry et al.*, 2009]. No method yet exists to assess subglacial discharge beneath either terrestrial or tidewater glaciers.

Seismic tremor produced by fluvial processes points toward an opportunity for measuring subglacial discharge [*Burtin et al.*, 2008, 2011; *Hsu et al.*, 2011; *Schmandt et al.*, 2013; *Gimbert et al.*, 2014]. This continuous, background tremor is characterized by low-amplitude seismic signals with durations of hours to months. Tremor spanning 0.5 to 9 Hz has been associated with water discharge across a range of fluxes and geologic settings, while higher frequencies are generated by bed load sediment transport [*Burtin et al.*, 2011; *Schmandt et al.*, 2013]. The relationship between water discharge and these higher, bed load transport frequencies exhibits hysteresis, consistent with supply-limited bed load transport [*Riihimaki et al.*, 2005; *Hsu et al.*, 2011; *Schmandt et al.*, 2013]. These studies suggest that turbulent water flow exerts time-varying shear and/or normal stress against the river bed, thereby generating seismic waves [*Gimbert et al.*, 2014]. These same mechanisms have the potential to generate detectable tremor within subglacial conduits at glacier beds.

2. Methods

2.1. Seismic Processing

To assess whether similar tremor signals are produced by subglacial discharge at the beds of glaciers in Alaska and Greenland, we analyze vertical channel, seismic recordings of ground velocity from stations

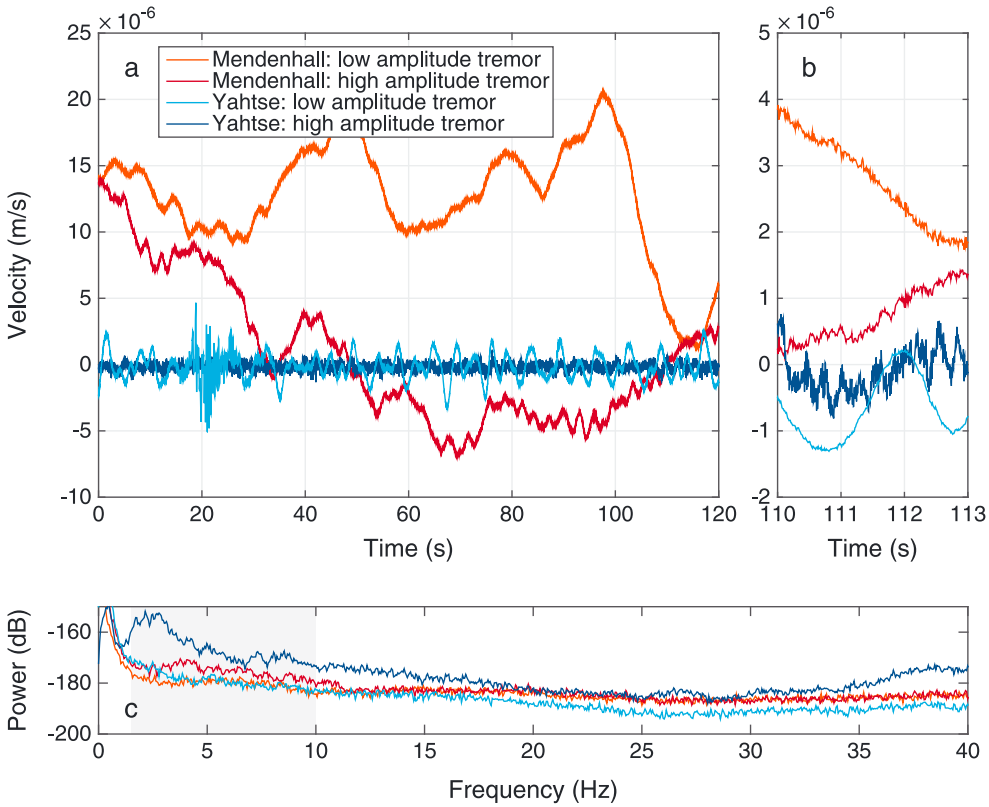

Figure 1. Seismic data from Mendenhall and Yahtse Glaciers, Alaska, during times with high- and low-amplitude > 0.5 Hz power. (a) Unfiltered waveforms recorded on the vertical channel of AMBR at Mendenhall (low amplitude: 3 June 2012; high amplitude: 1 August 2012) and LUPN at Yahtse Glacier (low amplitude: 3 January 2011; high amplitude: 6 August 2010). A typical icequake, produced by calving at Yahtse Glacier [*Bartholomaus et al.*, 2012], is recorded at 20 s during the low-amplitude period at Yahtse. (b) Blowup of Figure 1a showing appearance of high-frequency signal. (c) Median spectra for 10 min surrounding the time periods in Figure 1a. The occurrence of an icequake during the low-amplitude period at Yahtse Glacier does not increase its median power. Gray shading indicates the frequency band best associated with subglacial discharge. Spectra from longer time periods are shown in Figure S2. Movie S1 animates this figure.

installed on land within 5 km of glacier termini (Figure S1 in the supporting information). We draw on data from intermediate period and broadband seismometers with a flat frequency response between at least 0.3 and 10 Hz at Mendenhall Glacier, Yahtse Glacier, Columbia Glacier, Hubbard Glacier, and Yakutat Glacier in Alaska. Additionally, at Jakobshavn Isbræ, in Greenland, we use a short-period sensor with a natural frequency of 2 Hz.

We statistically characterize seismic "noise" (which includes tremor) by identifying the median power spectral density (PSD) within short-duration moving windows, subsampled from within a longer-duration waveform (Figure 1). To minimize the likelihood that a PSD samples a discrete event, such as an icequake or earthquake, and maximizes the number of individual PSDs, we use short-duration (20 s) waveforms with 50% overlap in all analyses. We then combine the short-duration PSDs to identify the probability that the power at a given frequency reaches a specific level during a longer-duration time window. Examples of these probabilistic representations (PSD-probability density functions) are shown in Figure S2 [*McNamara and Buland*, 2004]. Power is shown in decibel ($10\log_{10}((m/s)^2/Hz)$). At Mendenhall Glacier, where we assess the response of the median PSD to a short-duration flood during one season, we calculate the median power of PSDs within 50% overlapping, 0.5 h time windows. At Yahtse Glacier, and all other glaciers where we look for seasonal shifts in tremor amplitude, we calculate the median power for 50% overlapping 1 day time windows. Our conclusions do not differ when other time windows, including 30 min, are used. For example, when noisier 30 min results are smoothed and compared with 1 day results, differences in tremor amplitude are approximately normally distributed around a mean bias of 3%, with a standard deviation of 14% difference. For daylong time windows, 8638 twenty second PSDs are averaged for each median PSD. To identify the

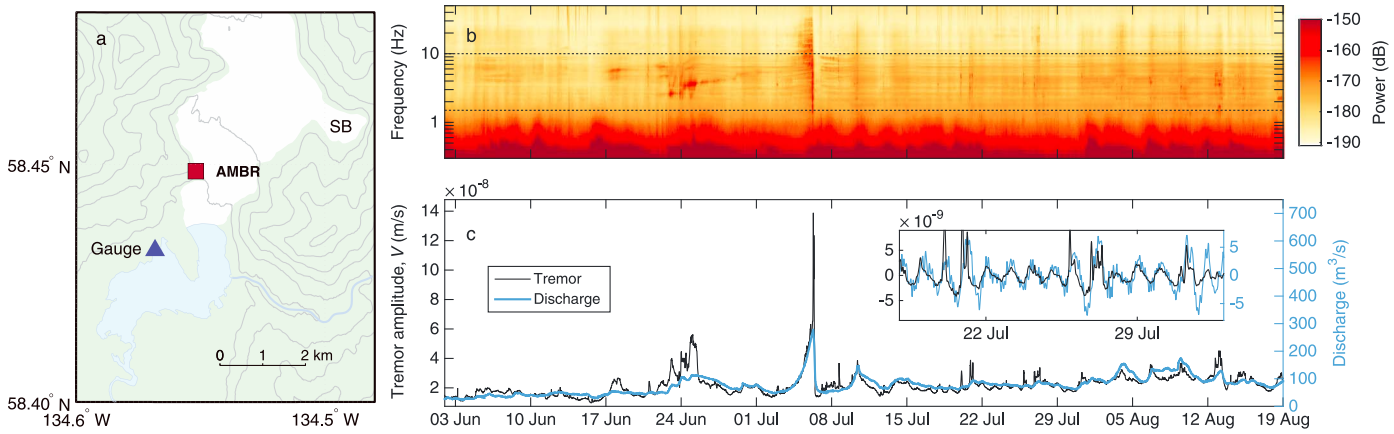

Figure 2. Glaciohydraulic tremor and discharge at Mendenhall Glacier, Alaska. (a) Map showing the terminus area of Mendenhall Glacier and Mendenhall Lake in which it terminates. SB is Suicide Basin, source of the 6 July flood. Nugget Creek enters Mendenhall Lake from the east. Locations of seismic station AMBR and the lake gage are marked. A second gage, not shown, records river discharge downstream of Mendenhall Lake. Contour lines are spaced every 200 m of elevation; Mendenhall Lake is at 16 m elevation. (b) Spectrogram developed from the median power of 30 min, 50% overlapping time windows of vertical channel seismic data from station AMBR, during 2012. The frequency range integrated to yield V in Figure 2c is bounded by dotted lines. (c) Tremor amplitude V and water discharge into Mendenhall Lake. Inset shows V and discharge band-pass filtered for periods between 2 h and 2 days.

glaciohydraulic tremor amplitude, we take the square root of the sum of the median PSD (with units of $(m/s)^2/Hz$) over specific frequencies of interest. As supported by the results described below, we select the range from 1.5 to 10 Hz. This integrated quantity is the tremor amplitude, V, which by Parseval's theorem is the median, absolute ground velocity between 1.5 and 10 Hz [*Press et al.*, 1988, p. 439].

2.2. Attribution of Tremor Source

We assess the possibility that glacier motion may generate tremor by comparing ice surface motion recorded by GPS with V recorded contemporaneously by seismometers. The GPS receivers at Mendenhall Glacier, IPA5 and WITE, were Trimble NetRSs installed near the glacier centerline (Figure S1). At Yahtse Glacier, station CNTR was a Trimble 5700 installed near the glacier centerline and above a near-terminus icefall (Figure S1). Data are postprocessed with the TRACK software [*Chen*, 1999] using base stations installed on bedrock as geodetic control. To arrive at velocities that can be directly compared with tremor amplitudes, we subsampled our data and differenced consecutive positions.

A U.S. Geological Survey stream and lake gaging program at lake-terminating Mendenhall Glacier allows us to identify the frequency range of seismic tremor that best correlates with water discharge while also minimizing bed load-produced hysteresis (Figure 2a). To calculate discharge into the lake Q_{in}, we apply mass conservation, $Q_{in} = Q_{out} + A\, dh/dt$, where Q_{out} is the gaged lake discharge, A is the lake area, and dh/dt is the rate of lake stage change. The only two significant sources for Q_{in} are Mendenhall Glacier and Nugget Creek. During a 4 year period while both Nugget Creek and Mendenhall River were gaged, Mendenhall Glacier contributed 60–90% of the summer discharge of Mendenhall River. Therefore, we assume that Nugget Creek and Mendenhall Glacier discharges covary and that Mendenhall River discharge variations (Figure 2) reflect variations in Mendenhall Glacier discharge. For a given discharge and V calculated as the integral over some frequency range, we classify the hysteresis as the mean width (minor axis) of convex hulls formed from the discharge and V grouped every 2 days over the course of the summer.

To examine the cooccurrence of peaks in V and water inputs to Yahtse Glacier, we combine local meteorological data with a temperature index melt model [*Hock*, 2003]. Using the mean, locally derived summer lapse rate, $0.0071°C\,m^{-1}$, and mean, daily, terminus air temperature, we calculate the elevation-dependent air temperature. We apply these temperatures to the glacier hypsometry and use the temperature index method to identify the timing of melt fluxes to the glacier surface with a midrange degree-day factor, $6 \times 10^{-3}\,m\,d^{-1}\,°C^{-1}$ [*Hock*, 2003]. To estimate rain inputs, we apply the precipitation rate measured at the glacier terminus to the lapse rate and hypsometry-calculated glacier area with air temperature above freezing. These melt and rain fluxes sum to the total modeled water input to Yahtse Glacier, shown respectively in red, blue, and gray in Figure 4d. While our model results may not reproduce the absolute

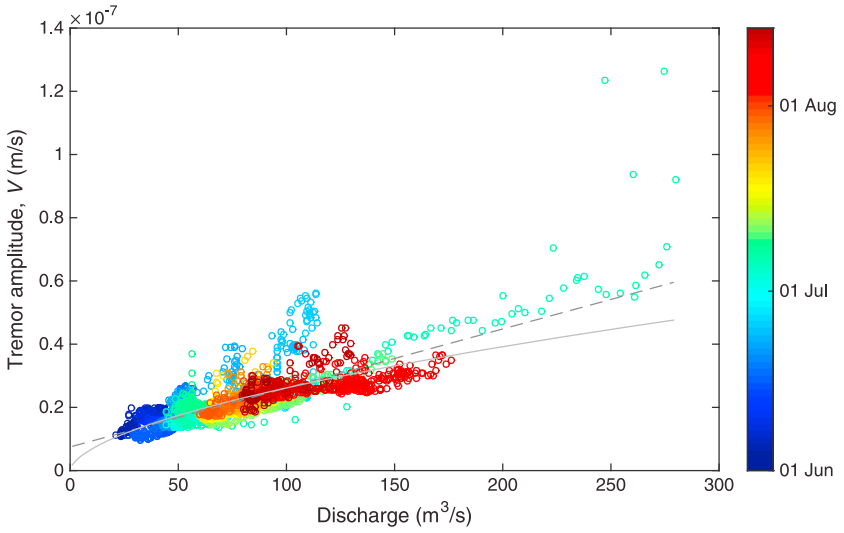

Figure 3. Relationship between discharge to Mendenhall Lake and tremor amplitude, V, between 1.5 and 10 Hz at Mendenhall Glacier. Here the data from Figure 2c are presented as a scatterplot. Tremor amplitude is recorded by station AMBR installed on bedrock within a kilometer of the glacier centerline. Color illustrates the date of 2012. Gray dashed line illustrates the least squares linear fit ($R^2 = 0.63$) between V and discharge, Q_{in}: $V = 1.9 \times 10^{-10} \times Q_{in} + 7.5 \times 10^{-9}$. Gray solid line illustrates the least squares fit $V = 1.7 \times 10^{-9} \times Q_{in}^{7/12}$ ($R^2 = 0.59$).

magnitude of water inputs, this approach accurately identifies the timing of peak water inputs to the glacier that are necessary for the evaluation of input-V lag times.

3. Results

We find that seismic noise recorded adjacent to glaciers varies over time and among glaciers (Figure 1). The clearest example of this is within the 0.05 to 0.5 Hz microseism band associated with storm intensity [*McNamara and Buland*, 2004], which at times dominates the spectra. In addition, the amplitudes at higher frequencies also vary. At Yahtse Glacier, midsummer power at 2.5 Hz is 20 dB greater than midwinter power. At Mendenhall Glacier, midsummer power at 4 Hz is 7 dB greater than early summer power. While transient events, such as icequakes and earthquakes, briefly increase the power >0.5 Hz within individual 20 s PSDs, such transient events are not required to produce amplified >0.5 Hz median power. Instead, strong, high-frequency ground motion at glaciers arises purely from the background noise from another, more slowly varying source (Figure 1 and supporting information Text S1 and Movie S1).

Simultaneous seismic, GPS, and discharge observations at Mendenhall Glacier allow us to evaluate potential seismogenic mechanisms. Time series of median spectra reveal power variations over hourly to weekly timescales, including in response to a glacial outburst flood on 6 July (Figure 2). As in Figure 1, the largest-amplitude signals are within the microseism band (0.05–0.5 Hz), but significant temporal variability is also present at higher frequencies. Discharge and seismic power >1.5 Hz track each other through a smooth, multiday increase prior to the flood peak. Immediately following peak discharge, seismic power abruptly increases for 3 h before both discharge and seismic power return to their preflood levels. The brief increase in seismic noise at the conclusion of the flood may reflect a swarm of basal icequakes produced by ice fracture when basal water pressures drop [*Walter et al.*, 2008]. Surface streams and moulins at Mendenhall Glacier are both smaller and more distant from the local seismic station than those producing tremor recorded on the Greenland Ice Sheet [*Röösli et al.*, 2014]. The GPS data reveal that these higher-frequency signals are not a product of ice flow (including basal motion) or longitudinal strain rate (Figures S3 and S4a). We find very little correlation between glacier motion and seismically recorded tremor amplitude ($r = 0.13$ at Mendenhall Glacier; all correlation coefficients are Pearson's; Figures S3 and S4). Instead, we do find a relationship between subglacial discharge from Mendenhall Glacier and >1 Hz tremor.

To identify the frequencies of seismic ground motion best associated with subglacial discharge, we maximize the linear relationship between tremor amplitude, V, within frequencies from 0.1 to 50 Hz and the discharge

to Mendenhall Lake. Tremor amplitude and discharge are best correlated ($r = 0.80$), with the least hysteresis, when V integrates frequencies between 1.5 and 10 Hz (Figures 2b and 3). At higher frequencies, we find that V is greater during rising discharge than during falling discharge—hysteresis compatible with bed load transport [*Burtin et al*., 2011; *Hsu et al*., 2011; *Schmandt et al*., 2013]. Below 1.5 Hz, we find no relationship. In midsummer, when subglacial drainage is expected to be efficient [*Chu*, 2013], we find that surface melt-driven diurnal variations in tremor amplitude and discharge are in phase (Figure 2c inset).

Additional evidence of glaciohydraulic tremor is found at Yahtse Glacier, a tidewater glacier in Alaska. With a network of nine broadband seismometers deployed off the ice but near the glacier perimeter, a GPS receiver, and a weather station (Figure 4a), we reassess our proposed source mechanism, test expectations of subglacial discharge, and identify areas of strongest tremor production. For each of 3 years and at each of the nine Yahtse Glacier stations, tremor amplitude increases sharply in June, reaches maximum levels up to tenfold greater than midwinter levels in August, and decays toward background winter levels in September (Figure 4c).

Although the temporal variations in tremor are similar among the nine seismic stations, their relative amplitudes vary. For 11 instances with peaks in V (generally associated with large rain events, when the signal-to-noise ratio is greatest), we normalized V for each station to that of station DOST (with the greatest median V) and calculated the median of the normalized values for each station (Figure 4a). Stations closest to an icefall, where Yahtse Glacier falls 700 m over 4 km, consistently record the largest-amplitude signals. However, as at Mendenhall Glacier, V is uncorrelated with glacier speed ($r = -0.17$), demonstrating that fast ice flow through the icefall is not the tremor source (Figure S4b). Icequakes have no meaningful effect on the median spectra (Figures 1 and S2). Rather, the time series of tremor amplitude resemble hydrographs from glacierized basins, including abrupt increases and slow decays in discharge (Figure 4c) [*Jansson et al*., 2003].

Local maxima in water inputs to Yahtse Glacier and tremor nearly coincide, with lags between input and V that decrease through the summer (Figure 4e). However, the amplitudes of individual peaks in V are not linearly related to the amplitude of their water inputs (Figures 4c and 4d), just as subglacial discharge does not necessarily correlate with melt and rain inputs [*Jansson et al*., 2003; *Chu*, 2013]. The lags between water input and V and the observation that tremor amplitude is greatest on both sides of the highly crevassed icefall (within which no surface streams or major moulins are found) eliminate supraglacial or englacial water as sources for the tremor [cf. *Röösli et al*., 2014]. Instead, the summer decrease in lag between water input and tremor amplitude supports the interpretation that Yahtse Glacier's subglacial hydrologic system evolves similarly to that of terrestrially terminating glaciers [*Jansson et al*., 2003]. Spring lags of 3–4 days are longer than those reported from dye injections directly into moulins [*Jansson et al*., 2003]. However, input-V lags may represent a more accurate characterization of the efficiency of the entire hydrologic system of Yahtse Glacier which, with its coastal location and high mean elevation, is characterized by a deep, early spring snowpack.

The similarity with tremor from Mendenhall Glacier, the diurnal to seasonal variation in V, decreasing lag times over the course of the summer, and the nonlinear response between water inputs and tremor amplitude lead us to suggest that subglacial discharge is the source of 1.5–10 Hz tremor. A physical model of turbulent water's time-varying drag against bed roughness in surface rivers predicts tremor within the 1.5–10 Hz range [*Gimbert et al*., 2014]. We propose that this mechanism is also responsible for the glaciohydraulic tremor signals we report here. By combining the predicted relationship between discharge and tremor amplitude from this model [*Gimbert et al*., 2014] with the commonly used Manning's equation for pipe flow [*Gulley et al*., 2012], we find that $V \propto Q^{7/12}$, where Q is the subglacial discharge (supporting information Text S2). The $V \propto Q^{7/12}$ model fits our data nearly as well as a linear model, with the added benefit of passing through the origin as one would expect if tremor is purely a function of discharge (Figure 3). Regardless of the exact relationship between seismic signals and discharge, our data empirically demonstrate that tremor can be used as a proxy for subglacial discharge.

We also find glaciohydraulic tremor in seismic data from Jakobshavn Isbræ, Greenland, and Columbia Glacier, Alaska (prior to ~2009, Figures S5 and S6). The peak frequencies at the four locations (Mendenhall, Yahtse, Jakobshavn, and Columbia) vary slightly but remain between 1.5 and 10 Hz (Figures 1, S5, and S6). Differences may result from contrasts in the size of subglacial conduits, contributions from higher-frequency

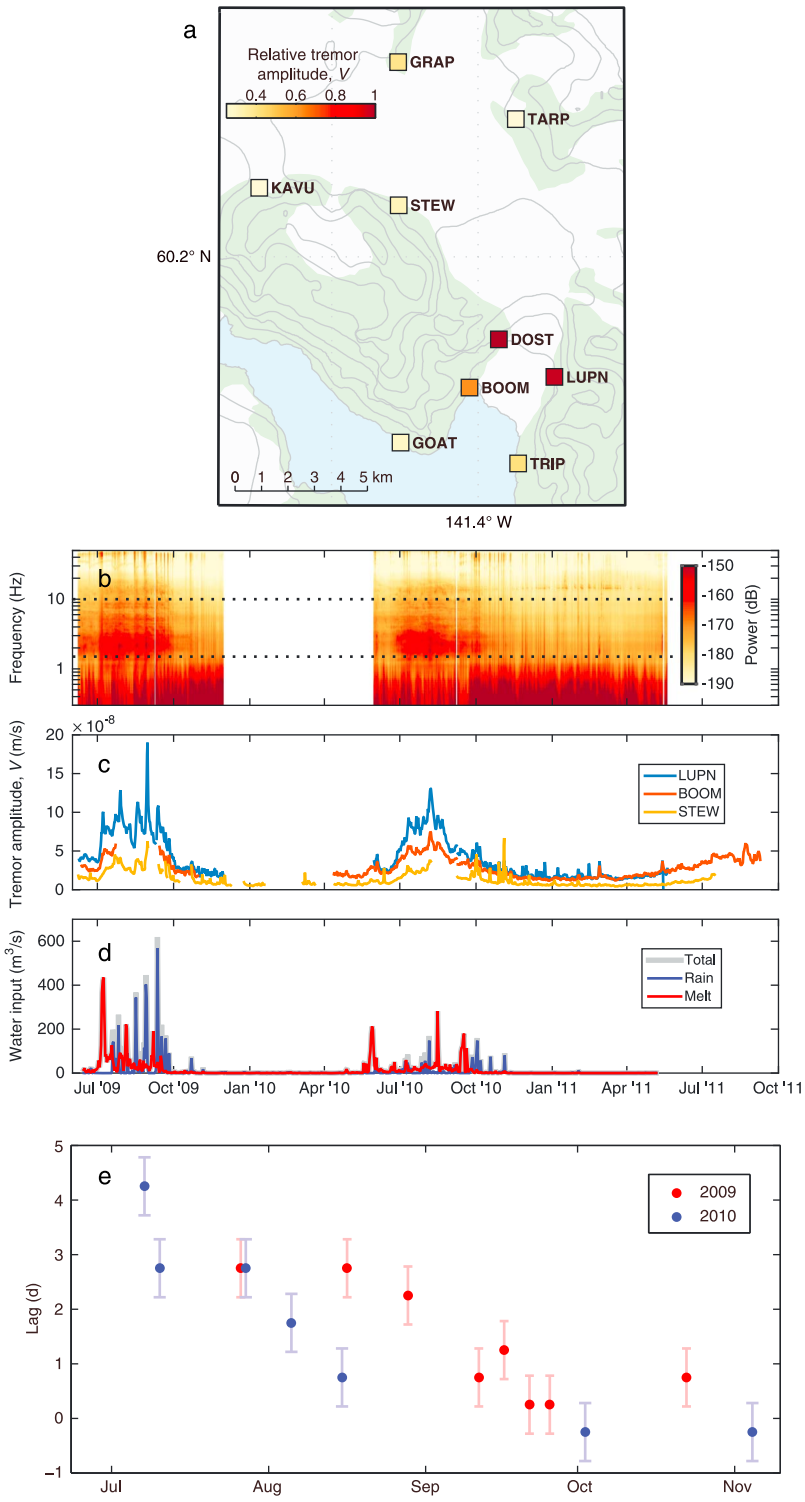

Figure 4. Glaciohydraulic tremor and water inputs to Yahtse Glacier. (a) Map of seismic stations surrounding the lower portion of Yahtse Glacier. Stations are color coded by their relative amplitudes during 11 times with maxima in *V*. Contour lines are spaced every 200 m of elevation. Yahtse Glacier flows through an icefall north of stations DOST and LUPN. (b) Spectrogram showing variations in background seismicity at station LUPN during our experiment. Gaps in records reflect instrument outages. (c) Tremor amplitude, *V*, integrated between 1.5 and 10 Hz (bounded by dotted lines in Figure 4b) for stations BOOM, LUPN, and STEW. (d) Estimates of water input from rain and ice melt during the 2009–2010 operational period of the terminus weather station. (e) Time lag between peak water input and peak glaciohydraulic tremor amplitude at Yahtse Glacier for 2009 and 2010. Shown are the 95% confidence limits for each lag.

bed load tremor, and preferential attenuation of high-frequency signals with increasing distance [*Tsai et al.*, 2012; *Gimbert et al.*, 2014]. Similar signals are absent at Yakutat Glacier or Hubbard Glacier, Alaska, or at Columbia Glacier after 2009 (Figures S7, S8, and S6). Through the use of a similar statistical characterization of seismic noise, *Walter et al.* [2010] also noted a decrease in 1.5–10 Hz power at Columbia Glacier between 2005 and 2009, which they attributed to a change in calving style. At Columbia Glacier, during the 2005–2009 time interval when the tremor signal vanished, the glacier terminus retreated from the seismometer, increasing the distance between the glacier centerline and the sensor from 1.7 km to 3.0 km (Figure S1). Similarly, the seismometers at Yakutat and Hubbard Glaciers are also >3 km from the grounded glaciers where subglacial discharge occurs. The dominant frequency and the amplitude of fluvial tremor both decrease sharply with increasing distance from the source [*Gimbert et al.*, 2014]. These two factors likely obscure glaciohydraulic tremor within the <1 Hz microseisms when observed from >3 km, such as at Columbia (post-2009), Yakutat, and Hubbard Glaciers. At Columbia Glacier between 2005 and 2009, increased attenuation of glaciohydraulic tremor is thus an alternate explanation for the reduction in 1.5–10 Hz power reported by *Walter et al.* [2010].

4. Discussion and Conclusions

Knowledge of the timing and occurrence of subglacial discharge is of fundamental importance for improved understanding and prediction of the ice mass loss at ice-ocean interfaces [*Straneo et al.*, 2013]. Yet even the seasonality of subglacial discharge is poorly known. Here we have presented the first confirmation of expected winter decreases in subglacial discharge beneath tidewater glaciers, based on observed decreases in glaciohydraulic tremor amplitude. *Meier and Post* [1987] suggested that the minimum water pressure at tidewater termini imposed by sea level could prevent the winter collapse of large-diameter conduits. The observed winter decrease in tremor amplitude indicates that subglacial discharge is limited more by melt and rainwater supply, in spite of this pressure minimum. During summer, high-amplitude tremor suggests that efficient conduits can be maintained at the beds of tidewater glaciers despite rapid basal motion that potentially disrupts their large diameters and ability to transmit water [*Meier and Post*, 1987]. At some of the fastest-flowing glaciers in Greenland, frictional melting at the glacier bed is estimated to make up 10–20% of the annual terrestrial runoff and maintain up to 100 m^3/s subglacial discharge during midwinter [*Echelmeyer et al.*, 1992; *Mernild et al.*, 2010]. While most of the seismic stations analyzed here suffered winter outages, future glaciohydraulic tremor observations may reveal the relative magnitudes of summer and winter discharge.

Seasonal variations in subglacial discharge may also explain observed summer terminus retreat at Yahtse and other glaciers [*Howat et al.*, 2010; *McNabb and Hock*, 2014] because submarine glacier melting is significantly enhanced by subglacial discharge [*Motyka et al.*, 2013; *Sciascia et al.*, 2013]. Our time series of glaciohydraulic tremor is consistent with submarine melt-driven terminus retreat, forced by summer subglacial discharge [*Ritchie et al.*, 2008].

The recent and abrupt mass losses from the Greenland and Antarctic ice sheets are driven in part by poorly understood processes acting at their marine margins [*Vieli and Nick*, 2011; *Nick et al.*, 2013; *Joughin et al.*, 2014]. Measurement of glaciohydraulic tremor can provide critical subglacial discharge data to better elucidate these processes, such as subsmarine melt [*Motyka et al.*, 2013; *Sciascia et al.*, 2013], calving, and fjord sedimentation [*Motyka et al.*, 2006]. These observations constitute evidence of the long-standing prediction that subglacial discharge through glaciers generates quantifiable seismic tremor [*St. Lawrence and Qamar*, 1979]. At present, seismology appears to be the only viable tool for studying the hourly to annual variations in subglacial discharge beneath tidewater glaciers. Furthermore, tremor observations can serve to validate models that route meltwater through and beneath tidewater glaciers. The presence of glaciohydraulic tremor at four different ocean- and lake-terminating glaciers indicates great promise for the widespread use of seismometers in oceanographic, geologic, ecological, and glaciological studies—wherever knowledge of freshwater discharge is needed but is otherwise obscured.

Acknowledgments

We thank the U.S. National Science Foundation for supporting data collection at Yahtse Glacier through grant EAR-0810313. T.C.B. was substantially supported by a postdoctoral fellowship from the University of Texas Institute for Geophysics. J.M.A. was supported by Alaska NASA EPSCoR Program (NNX13AB28A). S.O. was supported by the U.S. Geological Survey Climate and Land Use Change Mission and the U.S. Department of Interior Alaska Climate Science Center. Seismic instrumentation was provided by the PASSCAL polar program of the Incorporated Research Institutions for Seismology (IRIS). Jamie Bradshaw and Marci Beitch assisted in the Mendenhall Glacier data collection effort. Two anonymous reviewers helped to improve the manuscript. Seismic data used in this study are archived at the Incorporated Research Institutions for Seismology Data Management Center (IRIS DMC, http://www.iris.edu/dms/nodes/dmc/). Stream gaging data for the Mendenhall River and Nugget Creek are available though http://waterdata.usgs.gov/ak/nwis/dv/?site_no=15052500 and http://waterdata.usgs.gov/ak/nwis/dv/?site_no=15052495. Any additional data may be obtained from T.C.B. (tbartholomaus@ig.utexas.edu). Use of trade, product, or firm names is for descriptive purposes only and does not imply endorsement by the U.S. Government.

The Editor thanks Gordon Hamilton and an anonymous reviewer for their assistance in evaluating this paper.

References

Bartholomaus, T. C., C. F. Larsen, S. O'Neel, and M. E. West (2012), Calving seismicity from iceberg-sea surface interactions, *J. Geophys. Res.*, *117*, F04029, doi:10.1029/2012JF002513.

Burtin, A., L. Bollinger, J. Vergne, R. Cattin, and J. L. Nábělek (2008), Spectral analysis of seismic noise induced by rivers: A new tool to monitor spatiotemporal changes in stream hydrodynamics, *J. Geophys. Res.*, *113*, B05301, doi:10.1029/2007JB005034.

Burtin, A., R. Cattin, L. Bollinger, J. Vergne, P. Steer, A. Robert, N. Findling, and C. Tiberi (2011), Towards the hydrologic and bed load monitoring from high-frequency seismic noise in a braided river: The "torrent de St Pierre", French Alps, *J. Hydrol.*, *408*(1–2), 43–53, doi:10.1016/j.jhydrol.2011.07.014.

Chen, G. (1999), GPS kinematic positioning for the airborne laser altimetry at Long Valley, California, PhD dissertation, 173 pp., Massachussetts Institute of Technology, Cambridge, Mass.

Chu, V. W. (2013), Greenland Ice Sheet hydrology: A review, *Prog. Phys. Geogr.*, *38*(1), 19–54, doi:10.1177/0309133313507075.

Echelmeyer, K., W. D. Harrison, T. S. Clarke, and C. Benson (1992), Surficial glaciology of Jakobshavns Isbrae, West Greenland: Part II. Ablation, accumulation and temperature, *J. Glaciol.*, *38*(128), 169–181.

Gimbert, F., V. C. Tsai, and M. P. Lamb (2014), A physical model for seismic noise generation by turbulent flow in rivers, *J. Geophys. Res. Earth Surf.*, 2209–2238, doi:10.1002/2014JF003201.

Gulley, J. D., P. Walthard, J. Martin, A. F. Banwell, D. I. Benn, and G. Catania (2012), Conduit roughness and dye-trace breakthrough curves: Why slow velocity and high dispersivity may not reflect flow in distributed systems, *J. Glaciol.*, *58*(211), 915–925, doi:10.3189/2012JoG11J115.

Hock, R. (2003), Temperature index melt modelling in mountain areas, *J. Hydrol.*, *282*(1–4), 104–115, doi:10.1016/S0022-1694(03)00257-9.

Howat, I. M., J. E. Box, Y. Ahn, A. Herrington, and E. M. McFadden (2010), Seasonal variability in the dynamics of marine-terminating outlet glaciers in Greenland, *J. Glaciol.*, *56*(198), 601–613, doi:10.3189/002214310793146232.

Hsu, L., N. J. Finnegan, and E. E. Brodsky (2011), A seismic signature of river bedload transport during storm events, *Geophys. Res. Lett.*, *38*, L13407, doi:10.1029/2011GL047759.

Jansson, P., R. Hock, and T. Schneider (2003), The concept of glacier storage: A review, *J. Hydrol.*, *282*(1–4), 116–129, doi:10.1016/S0022-1694(03)00258-0.

Joughin, I., B. E. Smith, and B. Medley (2014), Marine ice sheet collapse potentially under way for the Thwaites Glacier basin, West Antarctica, *Science*, *344*, 735–738.

Lydersen, C., et al. (2014), The importance of tidewater glaciers for marine mammals and seabirds in Svalbard, Norway, *J. Mar. Syst.*, *129*, 452–471, doi:10.1016/j.jmarsys.2013.09.006.

McNabb, R. W., and R. Hock (2014), Alaska tidewater glacier terminus positions, 1948–2012, *J. Geophys. Res. Earth Surf.*, *119*, 1–15, doi:10.1002/2013JF002915.Tidewater.

McNamara, D. E., and R. P. Buland (2004), Ambient noise levels in the continental United States, *Bull. Seismol. Soc. Am.*, *94*(4), 1517–1527.

Meier, M. F., and A. Post (1987), Fast tidewater glaciers, *J. Geophys. Res.*, *92*(B9), 9051–9058, doi:10.1029/JB092iB09p09051.

Mernild, S. H., I. M. Howat, Y. Ahn, G. E. Liston, K. Steffen, B. H. Jakobsen, B. Hasholt, B. Fog, and D. van As (2010), Freshwater flux to Sermilik Fjord, SE Greenland, *Cryosphere*, *4*, 453–465, doi:10.5194/tc-4-453-2010.

Motyka, R. J., M. Truffer, E. M. Kuriger, and A. K. Bucki (2006), Rapid erosion of soft sediments by tidewater glacier advance: Taku Glacier, Alaska, USA, *Geophys. Res. Lett.*, *33*, L24504, doi:10.1029/2006GL028467.

Motyka, R. J., W. P. Dryer, J. Amundson, M. Truffer, and M. Fahnestock (2013), Rapid submarine melting driven by subglacial discharge, LeConte Glacier, Alaska, *Geophys. Res. Lett.*, *40*, 1–6, doi:10.1002/grl.51011.

Nick, F. M., A. Vieli, M. L. Andersen, I. Joughin, A. Payne, T. L. Edwards, F. Pattyn, and R. S. W. van de Wal (2013), Future sea-level rise from Greenland's main outlet glaciers in a warming climate, *Nature*, *497*(9171), 235–238, doi:10.1038/nature12068.

Press, W. H., B. P. Flannery, S. A. Teukolsky, and W. T. Vetterling (1988), *Numerical Recipes in C: The Art of Scientific Computing*, 1st ed., Cambridge Univ. Press, Cambridge, U. K.

Riihimaki, C. A., K. R. MacGregor, R. S. Anderson, S. P. Anderson, and M. G. Loso (2005), Sediment evacuation and glacial erosion rates at a small alpine glacier, *J. Geophys. Res.*, *110*, F03003, doi:10.1029/2004JF000189.

Ritchie, J. B., C. S. Lingle, R. J. Motyka, and M. Truffer (2008), Seasonal fluctuations in the advance of a tidewater glacier and potential causes: Hubbard Glacier, Alaska, USA, *J. Glaciol.*, *54*(186), 401–411.

Röösli, C., F. Walter, S. Husen, L. C. Andrews, M. P. Lüthi, G. A. Catania, and E. Kissling (2014), Sustained seismic tremors and icequakes detected in the ablation zone of the Greenland Ice Sheet, *J. Glaciol.*, *60*(221), 563–575, doi:10.3189/2014JoG13J210.

Schmandt, B., R. C. Aster, D. Scherler, V. C. Tsai, and K. Karlstrom (2013), Multiple fluvial processes detected by riverside seismic and infrasound monitoring of a controlled flood in the Grand Canyon, *Geophys. Res. Lett.*, *40*, 4858–4863, doi:10.1002/grl.50953.

Sciascia, R., F. Straneo, C. Cenedese, and P. Heimbach (2013), Seasonal variability of submarine melt rate and circulation in an East Greenland fjord, *J. Geophys. Res. Oceans*, *118*, 1–15, doi:10.1002/jgrc.20142.

Slater, D. A., P. W. Nienow, T. R. Cowton, D. N. Goldberg, and A. J. Sole (2015), Effect of near-terminus subglacial hydrology on tidewater glacier submarine melt rates, *Geophys. Res. Lett.*, *42*, 1–8, doi:10.1002/2014GL062494.

St. Lawrence, W., and A. Qamar (1979), Hydraulic transients: A seismic source in volcanoes and glaciers, *Science*, *203*(4381), 654–656, doi:10.1126/science.203.4381.654.

Straneo, F., et al. (2013), Challenges to understanding the dynamic response of Greenland's marine terminating glaciers to oceanic and atmospheric forcing, *Bull. Am. Meteorol. Soc.*, *94*(8), 1131–1144, doi:10.1175/BAMS-D-12-00100.1.

Tsai, V. C., B. Minchew, M. P. Lamb, and J.-P. Ampuero (2012), A physical model for seismic noise generation from sediment transport in rivers, *Geophys. Res. Lett.*, *39*, L02404, doi:10.1029/2011GL050255.

Vieli, A., and F. M. Nick (2011), Understanding and modelling rapid dynamic changes of tidewater outlet glaciers: Issues and implications, *Surv. Geophys.*, *32*, 437–458, doi:10.1007/s10712-011-9132-4.

Walter, F., N. Deichmann, and M. Funk (2008), Basal icequakes during changing subglacial water pressures beneath Gornergletscher, Switzerland, *J. Glaciol.*, *54*(186), 511–521, doi:10.3189/002214308785837110.

Walter, F., S. O'Neel, D. McNamara, W. T. Pfeffer, J. N. Bassis, and H. A. Fricker (2010), Iceberg calving during transition from grounded to floating ice: Columbia Glacier, Alaska, *Geophys. Res. Lett.*, *37*, L15501, doi:10.1029/2010GL043201.

Winberry, J. P., S. Anandakrishnan, and R. B. Alley (2009), Seismic observations of transient subglacial water-flow beneath MacAyeal Ice Stream, West Antarctica, *Geophys. Res. Lett.*, *36*, L11502, doi:10.1029/2009GL037730.

Geophysical Research Letters

Supporting Information for

Subglacial discharge at tidewater glaciers revealed by seismic tremor

Timothy C. Bartholomaus[1], Jason M. Amundson[2], Jacob I. Walter[1], Shad O'Neel[3], Michael E. West[4] & Christopher F. Larsen[4]

[1]University of Texas, Institute for Geophysics, Austin, Texas, USA
[2]University of Alaska Southeast, Department of Natural Sciences, Juneau, Alaska, USA
[3]Alaska Science Center, U.S. Geological Survey, Anchorage, Alaska, USA
[4]University of Alaska Fairbanks, Geophysical Institute, Fairbanks, Alaska, USA

Contents of this file

Additional Supporting Information (Files uploaded separately)

Introduction

Text, figures and movie included in this supplement provide additional information supporting the conclusions of the main text.

Text S1. Median power spectral density as a characterization of background seismic signals

While Fig. 1 presents the appearance of unfiltered, raw waveform data, Fig. S2 demonstrates that patterns of seismic power differ over time periods longer than the relatively short durations shown in Fig. 1. Individual power spectral densities (PSDs) of 20 s samples can vary substantially, for example, reaching the levels identified as "maximum power" during brief, transient seismic events like calving icequakes and earthquakes. However, the majority of the 8,638 PSDs combined within each panel of Fig. S2 follow patterns that are distinct between summer and winter. For example, at 2 Hz, the middle 50% of summer PSDs fall between -159 and -151 dB, whereas the middle 50% of winter PSDs attain much lower 2 Hz power levels: between -179 and -167 dB.

In Fig. S2 and elsewhere throughout this manuscript, these distinct patterns are characterized by the median power level during specified time windows. During summer, median power at frequencies >1 Hz is up to 20 dB greater than during winter and is characterized by several clearly-defined local maxima, including particularly elevated power from 1.5 to 10 Hz. This frequency range includes the dominant frequency of calving-generated icequakes, the most common seismic events recorded on the Yahtse Glacier network [*Bartholomaus et al.*, 2012]. However, even at Yahtse Glacier, which produces anomalously high numbers of calving icequakes [*O'Neel et al.*, 2010], transient seismic events such as icequakes or earthquakes make up only 13% of the operational record of a seismometer adjacent to the glacier terminus [*Bartholomaus*, 2013]. Experiments performed by altering 13% of mid-summer PSDs to extremely high or low power levels only alters the median PSD at 2 Hz by 1 dB, far less than the seasonal difference of 20 dB. Thus, our median-based approach is largely insensitive to discrete events.

Furthermore, the median power during summer calving-free times at Yahtse Glacier, with no transient events in the waveform, has a structure strikingly similar to that of the summer 1-day median. Nearly identical patterns are present for any summer period selected at random, demonstrating that the median PSD structure during times with high tremor amplitude arises directly from the background noise. Thus, we conclude that the tremor we report here is due to a long-lived background process, not the result of high amplitude transient events.

Bartholomaus, T. C. (2013), Seismicity, seawater and seasonality: new insights into iceberg calving from Yahtse Glacier, Alaska, Ph.D. dissertation, Dept. of Geol. and Geophys., Univ. of Alaska Fairbanks, Fairbanks, Alaska, USA.

O'Neel, S., C. F. Larsen, N. Rupert, and R. Hansen (2010), Iceberg calving as a primary source of regional-scale glacier-generated seismicity in the St. Elias Mountains, Alaska, *J. Geophys. Res.*, *115*(F4), 1–12, doi:10.1029/2009JF001598.

Text S2. Covariation between subglacial discharge and tremor amplitude

We have hypothesized that time-varying drag, produced by turbulent subglacial discharge past roughness at glacier beds, produces the tremor signals we report here [*Gimbert et al.*, 2014]. For this mechanism, the seismic power at a given location depends in part on the shear velocity raised to the 14/3 power (equations 32 and 43 of *Gimbert et al.*, [2014]); shear velocity is generally considered to be a fixed fraction of the mean flow velocity, u. The Manning equation, which has often been used to estimate flow speed within subglacial conduits [*Gulley et al.*, 2012], predicts

$$u = \frac{R_h^{2/3} S^{1/2}}{n}$$

where R_h is the hydraulic radius, S is the hydraulic gradient, and n is the Manning roughness. Re-organizing Manning's equation and assuming that the cross-sectional area of the subglacial conduit is proportional to R_h^2 reveals that $u \propto Q^{1/4}$. Thus, seismic power $\propto Q^{7/6}$. V is the square root of the integrated power, so $V \propto Q^{7/12}$.

The relationship $V \propto Q^{7/12}$ can be approximated as linear with ≤6% error in V for a doubling or halving of Q. Model misfits this small are not resolved by our data. Regardless, our data, which exhibit a strong link between V and Q, provide support for the proposed mechanism [*Gimbert et al.*, 2014]. Both linear and 7/12th relationships between V and Q are shown in Fig. 3.

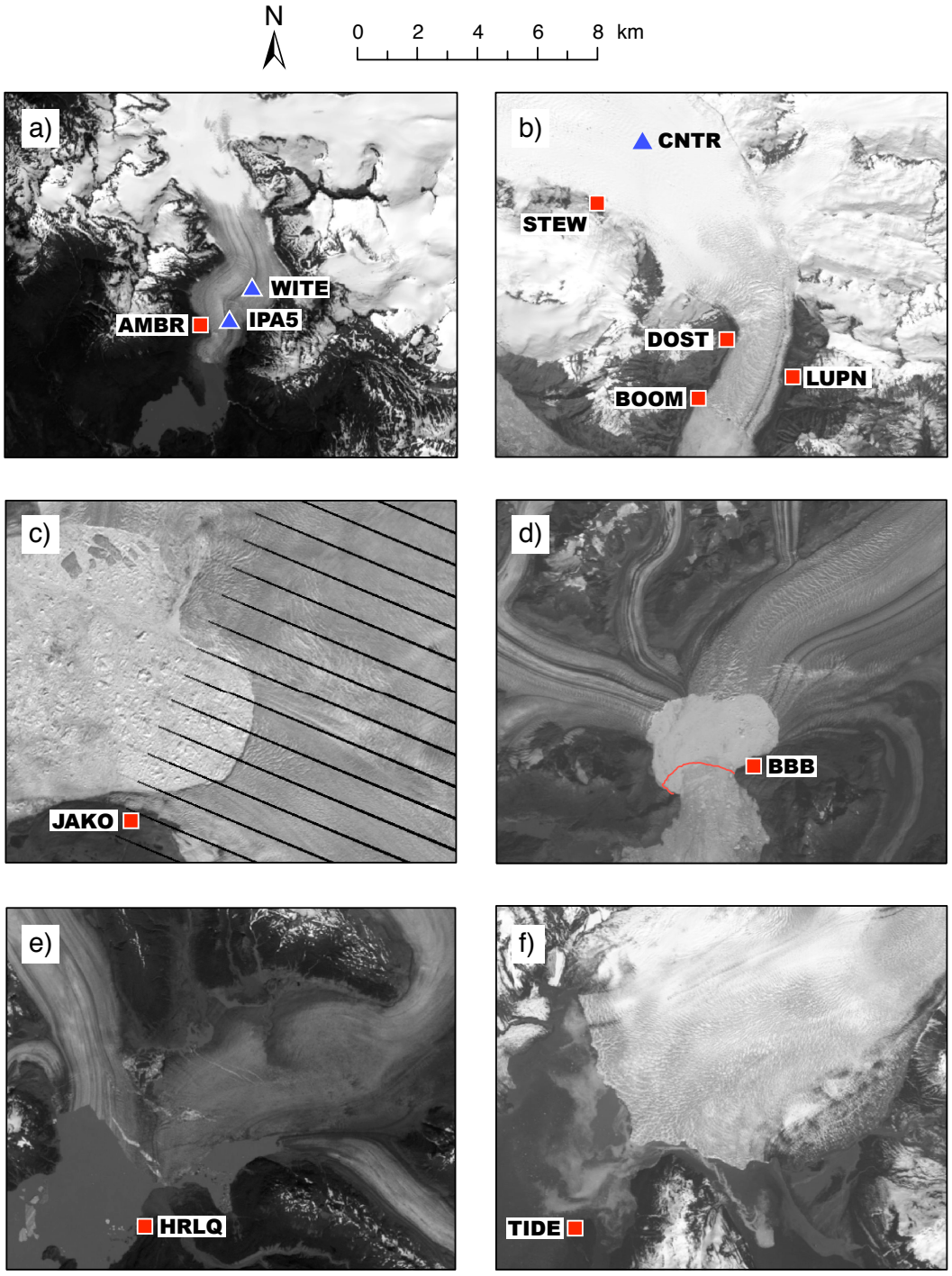

Figure S1. Landsat scenes of the terminus regions of each of the 6 glaciers discussed in this study. All images are displayed at the same scale. Images courtesy of U.S. Geological Survey (http://landsatlook.usgs.gov/). Seismometer locations are marked with red squares. a) Mendenhall Glacier on 30 June 2013. The locations of the GPS stations discussed here are marked with blue triangles. b) Yahtse Glacier on 9 June 2009. Four of nine Yahtse Glacier seismometers shown. GPS station is identified with a blue triangle. c) Jakobshavn Isbræ on 25

August 2007. d) Columbia Glacier on 6 September 2009. Red line shows the location of the terminus on 19 July 2006, prior to the terminus' separation from the bedrock headland on which BBB was installed. e) Yakutat Glacier on 14 August 2010. Yakutat Glacier has a significant floating tongue; HRLQ is approximately 5 km from the grounding line. f) Hubbard Glacier on 9 June 2009.

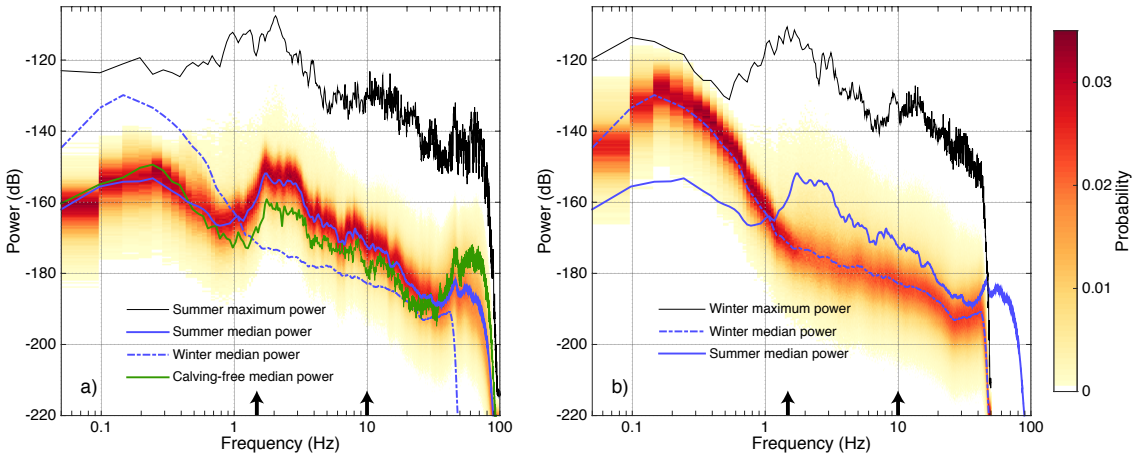

Figure S2. Seasonal contrasts in spectra at Yahtse Glacier, Alaska. Power spectral density-probability density functions (PSD-PDFs) from station LUPN for two days representative of summer and winter: (a) 6 Aug. 2010 and (b) 3 Jan. 2011. Other, summer and winter choices have similar PSD-PDFs. Color scale shows the probability of a PSD for an individual, 20 s sample of seismic waveform reaching a specific power level. Overlying the PSD-PDFs are the median power for the day, the median power for the other day (to facilitate comparison), and the maximum power level, per frequency, of any 20 s PSD. (a) also shows the median power of 5 min on 7 September 2010 during which no calving events, icequakes or earthquakes occurred. Arrows identify the bounds of the 1.5-10 Hz range which is integrated to produce the time series of tremor amplitude, *V*. The Nyquist frequency varied between 50 Hz during the winter and 100 Hz during the summer.

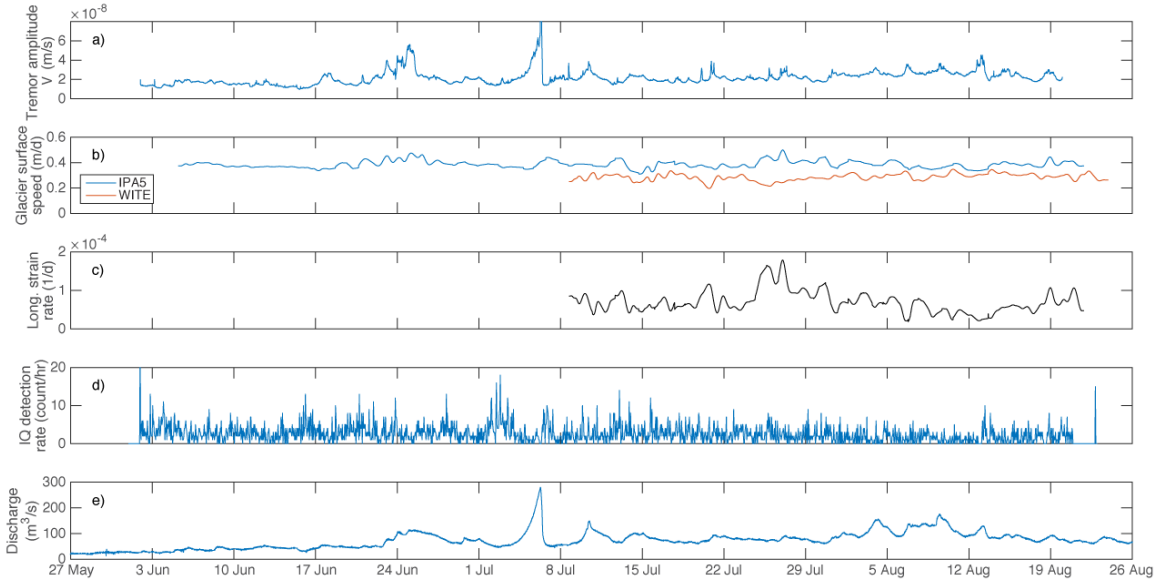

Figure S3. Comparison between tremor amplitude, glacier motion, icequake rate, and subglacial discharge during 2012. a) Tremor amplitude recorded by station AMBR, as in Fig. 2c. b) Mendenhall Glacier horizontal surface speed recorded by GPS at IPA5 and WITE (location on Fig. S1). c) Longitudinal strain rate between IPA5 and WITE. d) Detection rate of icequakes. e) Rate of discharge to Mendenhall Lake, as in Fig. 2c. Icequakes are detected using a short-term average/long-term average (STA/LTA) detector with a 0.2 s short term window and a 30 s long term window, bandpass filtered between 1.5 and 10 Hz, with a signal to noise detection threshold of 5, applied to the vertical channel of AMBR. We varied the detector parameters (for example, a STA window of 0.5s and a LTA window of 10 s) and identify no qualitative difference in the resulting pattern of detection rate. Because the long-term average seismic amplitude varies over time, the threshold for icequake detection also varies. During time intervals with high tremor amplitude, such as during the flood on July 6, not all icequakes may be detected.

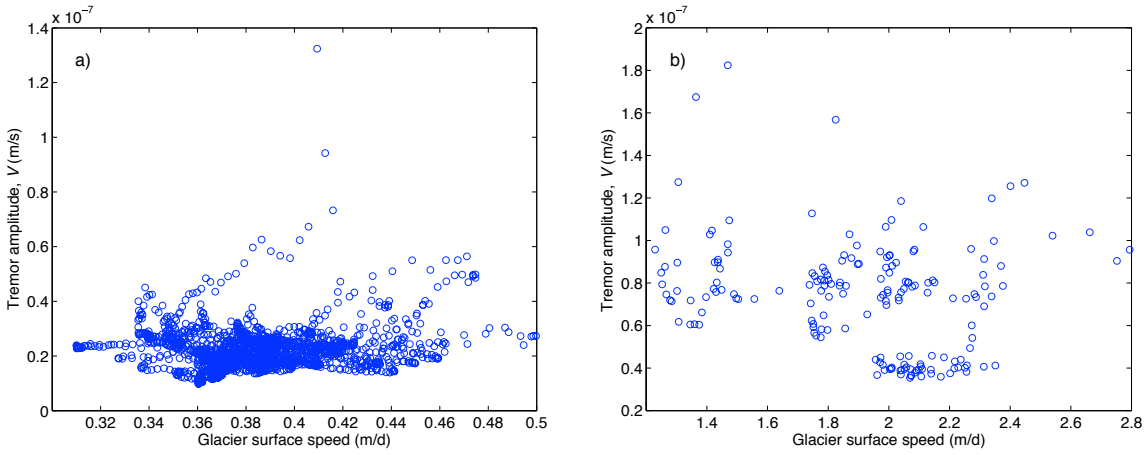

Figure S4. Comparison between glacier surface speed and tremor amplitude. a) Mendenhall Glacier surface speed recorded by GPS at IPA5 (location on Fig. S1) and tremor amplitude *V*, recorded at AMBR during summer 2012. b) Yahtse Glacier surface speed recorded by GPS at CNTR (location on Fig. S1) and tremor amplitude *V*, recorded at LUPN mid-June to mid-September of 2009.

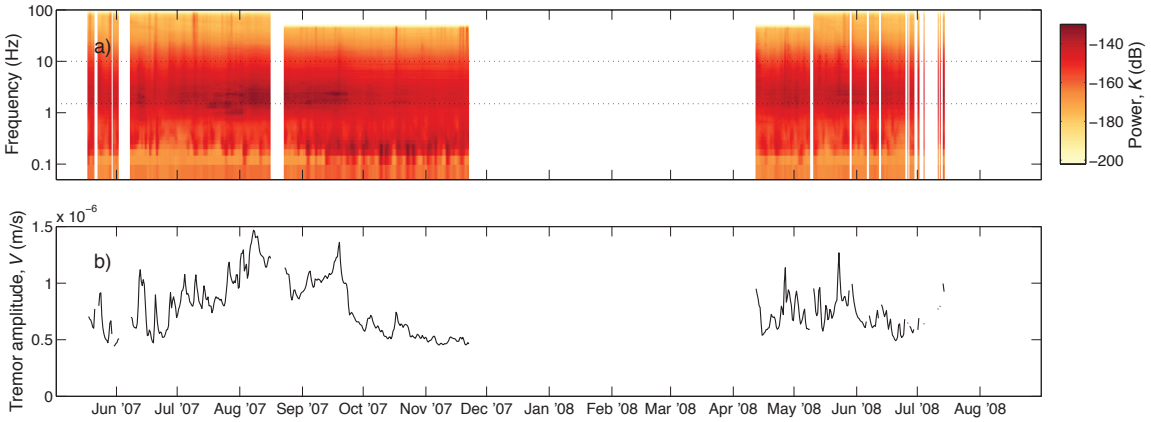

Figure S5. Tremor recorded at Jakobshavn Isbræ, Greenland. Station is JAKO, an L-22 short-period sensor, running from 2007 to 2008. a) Spectrogram constructed from the median power of 50% overlapping, 24 h time windows, as in Fig. 4. b) Tremor amplitude over the frequency range 1.5 to 10 Hz, drawing on the median powers of (a). Gaps in the record result from instrument outages.

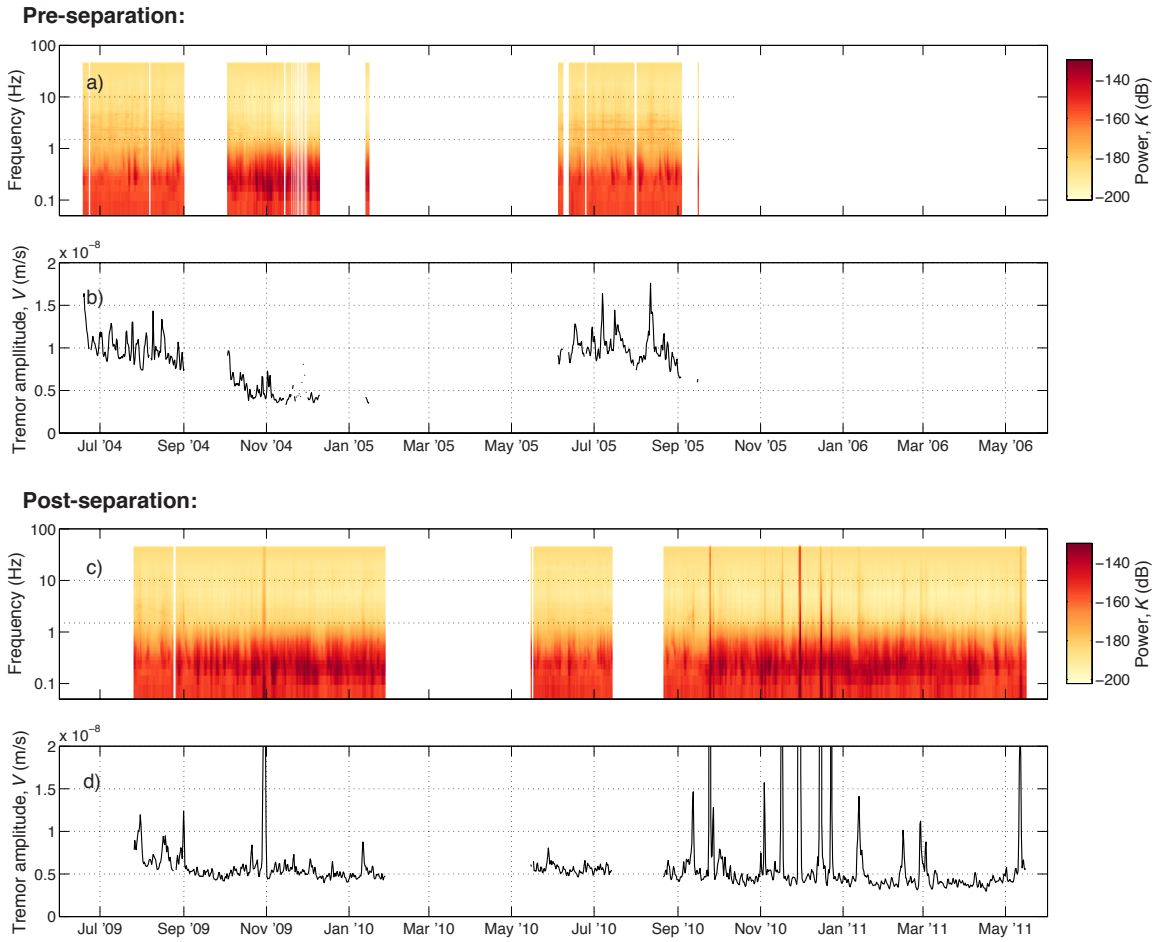

Figure S6. Tremor recorded at Columbia Glacier, Alaska. Station is BBB, a CMG-40T intermediate period seismometer, installed from 2004 to 2005 and again from 2009 to 2011. Between 2005 and 2009, the terminus of Columbia Glacier separated from the bedrock headland on which BBB was installed and opened a deep bay between BBB and the terminus (Fig. S1). a) Spectrogram constructed from the median power of 50% overlapping, 24 h time windows, as in Fig. 4, for the pre-separation period. b) Tremor amplitude over the frequency range 1.5 to 10 Hz, drawing on the median powers of (a). c, d) As for (a) and (b), but for the time period following the glacier's separation.

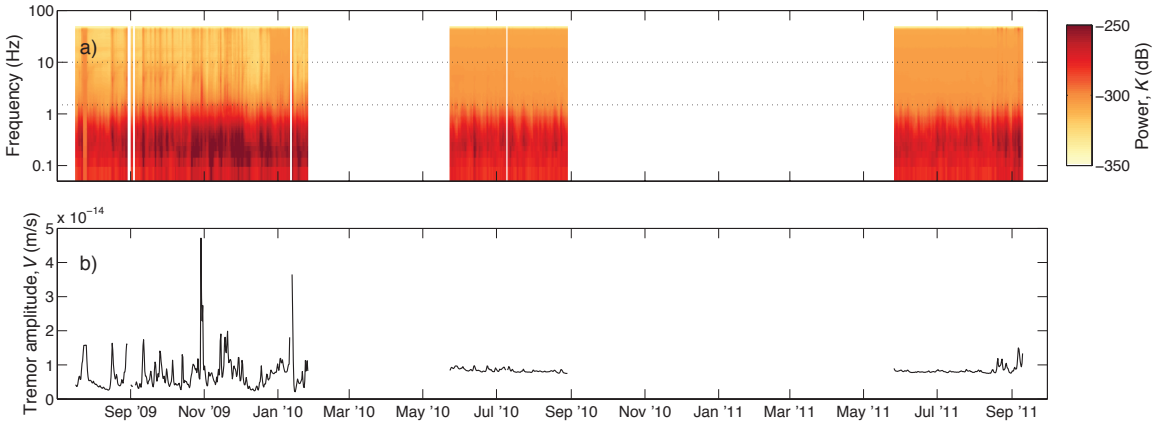

Figure S7. Tremor recorded at Yakutat Glacier, Alaska. Station is HRLQ, an STS-2 broadband seismometer, installed from 2009 to 2011. a) Spectrogram constructed from the median power of 50% overlapping, 24 h time windows, as in Fig. 4. b) Tremor amplitude over the frequency range 1.5 to 10 Hz, drawing on the median powers of (a).

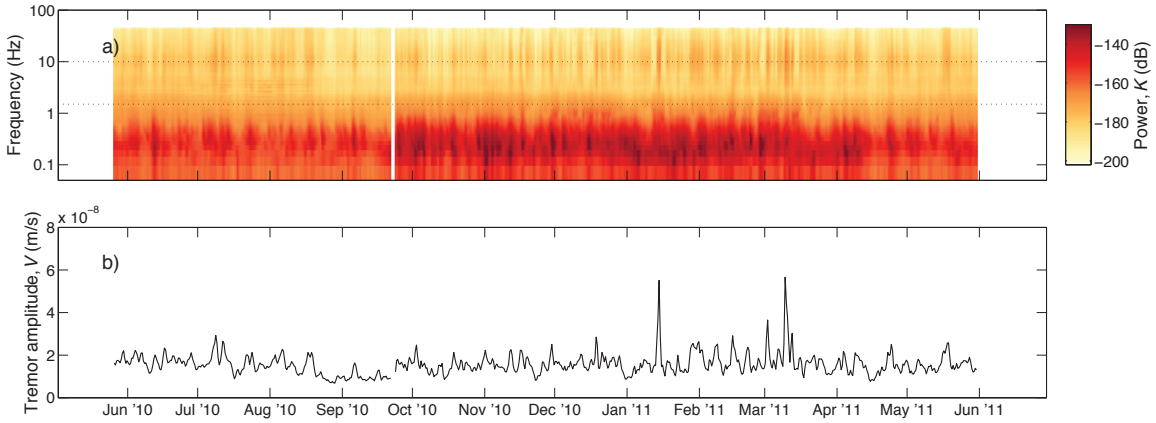

Figure S8. Tremor recorded at Hubbard Glacier, Alaska. Station is TIDE, a CMG-3T broadband seismometer, installed from 2010 to 2011. a) Spectrogram constructed from the median power of 50% overlapping, 24 h time windows, as in Fig. 4. b) Tremor amplitude over the frequency range 1.5 to 10 Hz, drawing on the median powers of (a).

Movie S1. Unfiltered seismic data and 20 s PSDs used to produce median spectra. These data are an animated version of Figure 1. Seismic data is from the vertical channel of station LUPN at Yahtse Glacier, Alaska. Red traces are from the summer (6 Aug 2010) and blue traces are from the winter (3 Jan 2011). As the seismic data scrolls (MM:SS), PSDs of 20 s subsamples of the data within the vertical black bars are presented on the right. Typical icequakes (produced by calving at the Yahtse Glacier terminus) briefly increase the power of individual PSDs, but most PSDs during the summer and during the winter have a similar character. This similar character is captured by the median spectra used in this study.